

Received November 2, 2019, accepted November 17, 2019, date of publication November 19, 2019,
date of current version December 2, 2019.

Digital Object Identifier 10.1109/ACCESS.2019.2954459

A Robotic Peg-in-Hole Assembly Strategy Based on Variable Compliance Center

SEN WANG^{ID}¹, GUODONG CHEN^{ID}¹, HUI XU^{ID}¹, AND ZHENG WANG^{ID}^{1,2}

¹Jiangsu Provincial Key Laboratory of Advanced Robotics, School of Mechanical and Electric Engineering, Soochow University, Suzhou 215123, China

²Shanghai Jiaotong University Affiliated Sixth People's Hospital, Shanghai Jiaotong University, Shanghai 200233, China

Corresponding authors: Zheng Wang (wangzheng6th@163.com) and Guodong Chen (guodongxyz@163.com)

This work was supported in part by the National Natural Science Foundation of China under Grant U1509202, and in part by the Key Project of Universities of Jiangsu Province in Natural Science Research under Grant 17KJA46007.

ABSTRACT Many kinds of peg-in-hole assembly strategies for an industrial robot have been reported in recent years. Most of these strategies are realized by utilizing visual and force sensors to assist robots. However, complex control algorithms that are based on visual and force sensors will reduce the assembly efficiency of a robot. This issue is thoughtless in traditional assembly strategies but is critical to further improve the efficiency of assembly automation. In this work, a new assembly strategy that is based on a displacement sensor and a variable compliant center is proposed to improve robot performance in assembly tasks. First, an elastic displacement device for this assembly strategy is designed, and its performance is analyzed. The displacement signal generated by the displacement sensor is used to detect the contact state of the peg and hole and to guide the robot to adjust the posture. Second, an assembly strategy, including the advantages of passive compliance and active compliance, and a simple assembly control system are designed to improve the assembly efficiency. Last, the effectiveness of the proposed assembly method is experimentally verified using a robot with 6 degrees of freedom and a chamferless peg and hole with a small clearance (0.1 mm). The experimental results show that the assembly strategy can successfully complete the precision peg-in-hole assembly and assist the robot in accurate assembly in industrial applications.

INDEX TERMS Peg-in-hole assembly, assembly strategy, compliant center, displacement sensor, elastic displacement device.

I. INTRODUCTION

In industrial production, assembly costs account for more than 50% of the total cost. With the development of industrial robots, robots are expected to replace the manual work required to complete assembly tasks. However, the application of robots to the precision assembly work is challenging. Considering the precision peg-in-hole assembly as an example, when the tolerance between a peg and hole is less than 0.1 mm, the improper adjustment caused by the initial positional deviation of the peg and hole may cause the failure of the assembly; the peg may fail to enter the hole or become stuck in the hole. In either case, the assembly workpiece or robot may be damaged. Due to the low repositioning precision of a robot in a precision peg-in-hole assembly, assembly with conventional position control is impossible. Eliminating the deviation of a workpiece position by robot

The associate editor coordinating the review of this manuscript and approving it for publication was Okyay Kaynak^{ID}.

teaching and visual localization is difficult. To solve this problem, compliant control methods are employed in robotic assembly tasks.

The first type of compliant control is passive compliant control that uses a special mechanical structure, such as a spring or a damping mechanism, to make a peg perform a passive compliance movement under external forces. For example, the RCC (remote center compliance) concept was first proposed by the Charles Stark Draper Laboratory at MIT in 1976 [1]. RCC was used to assist robots in overcoming position errors in the assembly process. Zhao and Wu [2] designed a variable remote center compliance device(VRCC) that can successfully complete an assembly task. Lee [3] improved the VRCC and simplified the mechanical structure of the VRCC to improve assembly efficiency. Park *et al.* [4] designed a new passive compliant device with a displacement measurement system and proposed a robotic assembly strategy to improve the performance of the robotic assembly system. A passive compliant assembly does not require a

complicated control system. However, this method has many disadvantages. Each assembly part needs to be designed with a separate compliant device. The method has strong specificity but poor adaptability and cannot be applied without any limitations.

The second type of control is active compliant control. A robot uses external sensors to sense the external environment and uses appropriate control strategies to adjust a pose to complete an assembly task based on the feedback information. One of the active compliance control methods is impedance control. Hogan [5] first proposed impedance control in 1985. Li *et al.* [6] proposed neural networks impedance control for robot-environment interaction. Krüger *et al.* [7] successfully completed a multiarm robot assembly using impedance control. Roveda *et al.* [8], [9] designed an optimal impedance force-tracking controller to obtain the performance of partially unknown contact environment properties even with errors in the initial estimate of the environment stiffness. Flores-Abad *et al.* [10] proposed a disturbance-based impedance controller for the compliance capture of an object using a free floating robot. Zeng *et al.* [11] used impedance control as the control outer loop to complete a peg-in-hole assembly task. Impedance control is highly flexible; however, the accurate rigidity and precise position of a constrained environment are required. The end force cannot be well controlled.

Other active compliant control methods are hybrid force/position control and parallel force/position control. Raibert and Craig [12] first proposed hybrid force/position control in 1981. Giblin *et al.* [13] used hybrid force/position control to insert a peg into hole at a faster rate with less friction force. Fang *et al.* [14] improved the hybrid force position control method to ensure correct assembly deformation and improve assembly quality. Ma *et al.* [15] used force-position hybrid control to control the contact force between a robot and the external environment and successfully completed the precision assembly of optical components. Hybrid force /position control can improve the control of the end force and satisfy the requirements of high-precision assembly tasks. However, solving the coupling of force control and position control is difficult. Therefore, many scholars have investigated parallel force/position control. Chiaverini and Sciavicco [16] first proposed parallel force/position control in 1988. Flixeder *et al.* [17] discussed the parallel force/position control system stability and an inner position control loop for friction compensation. Chen *et al.* [18] proposed a robust adaptive position/force control algorithm based on the parallel force/position control algorithm, which was able to adequately track the desired posture and force. Unlike hybrid force/position control, in parallel force/position control, the force control and output of the position controller are coincident and act in the same direction. However, this control is too complicated and the work efficiency is low.

In addition, some robotic intelligent assembly control methods have been extensively investigated by many scholars

in recent years. Jakovljevic *et al.* [19] proposed a fuzzy inference mechanism for recognizing contact states of a peg and hole. Inoue *et al.* [20] successfully applied deep reinforcement learning to high-precision assembly tasks. Xu *et al.* [21] proposed a model-driven deep deterministic policy gradient algorithm to accomplish the dual peg-in-hole assembly task through the learned policy without analyzing the contact states. Fan *et al.* [22] proposed a learning framework that combines both the supervised learning and the reinforcement learning, which realized a high precision industrial assembly. Lee *et al.* [23] applied self-supervised learning to fuse vision and touch and successfully completed different shapes of peg and hole assembly tasks. Although the intelligent assembly control method can successfully complete a robot assembly task, its stability and efficiency are low. Therefore, many intelligent control methods remain in the simulation stage, and their application in industry is difficult.

To simplify assembly control systems, improve assembly efficiency and reduce system cost, we propose an assembly strategy that is based on variable compliance centers. Compliance center is defined as a point on a compliant mechanism that has the ability to passively comply with external forces and torques. In this paper, we set the TCP (Tool Center Point) of the robot as the compliance center. The variable compliance center is position of the TCP changes on the axis of an assembly peg.

The contributions of this paper are described as follows: 1) the design of a compliant device for peg-in-hole assembly tasks; 2) the proposal of a new peg-in-hole assembly strategy based on the variable compliant center; and 3) the solution of the problem of assembly failure caused by assembly peg tilt and assembly peg and hole positioning error during robot assembly.

This paper is organized as follows. In Section II, the components and performance of the elastic displacement device are introduced and analysed. In Section III, we propose the assembly strategy by analyzing the contact state of the peg-in-hole. In Section IV, the control frameworks for the peg-in-hole assembly is designed. In Section V, the assembly error is theoretically analyzed. In Section VI, to verify the proposed assembly strategy, peg-in-hole assembly experiments are presented by using a 6 degree of freedom (DOF) robot, peg and hole with a tolerance of 0.1 mm. In Section VII, we compare and analyze the propose assembly strategy with the current classical assembly strategy. Section VIII gives the conclusions of this paper.

II. ELASTIC DISPLACEMENT DEVICE

A. PROPOSED MECHANISM

The main components of the elastic displacement device are shown in FIGURE 1. The spring is used to store the energy generated by the displacement. The displacement sensor is used to measure the displacement generated by the assembly peg during the assembly tasks. The ball spline is used to limit the twisting of the upper and lower ends of the device to ensure so that the device has only one degree of freedom.

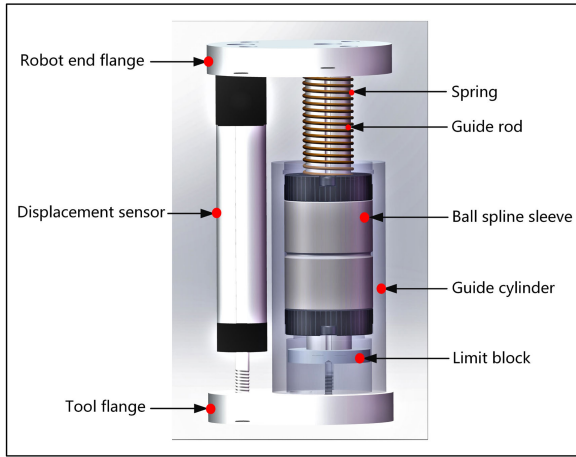


FIGURE 1. Elastexttic displacement device.

TABLE 1. Performance parameters of elastic displacement device.

Performance	Force	Stroke	Precision	Response Time
Actual Value	5 N-15 N	19 mm	0.01 mm	18 ms

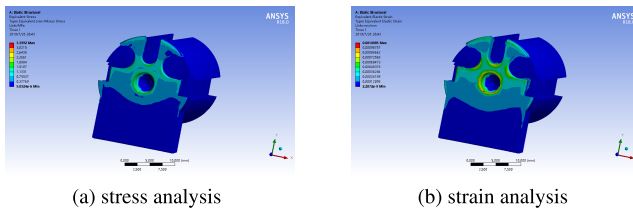


FIGURE 2. Strength analysis diagram of the top of the displacement sensor.

The equipment is employed in the assembly strategy of the variable compliant center, which is installed at the end of the industrial robot. When the robot starts to assemble, the compliant center of the assembly peg will change due to the spring's elasticity, and the displacement sensor will generate a signal to determine the contact state of the peg and hole. It has the advantages of simple structure and control, low cost of production and short of response time; its performance is listed in Table 1.

B. ANALYSIS OF THE PROPOSED MECHANISM

We use the ANSYS simulation analysis software to analyze the strength of the key components of the compliant device. According to the design requirements, a stress and strain analysis were carried out under the action of 300 N.m torque and 500 N axial force. A simulation analysis of the key components is shown in FIGURE 2, 3, 4, and 5.

The simulation results in Table 2 indicate that the key components of the compliant device cause slight deformation and stress in the designed working conditions, have minimal influence on the performance of the compliant device and can satisfy the actual working requirements.

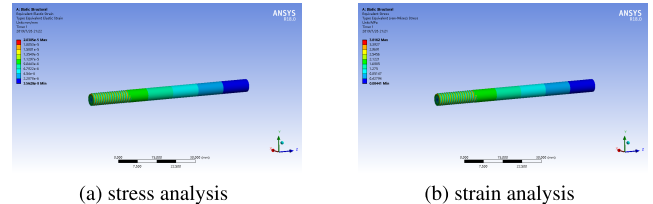


FIGURE 3. Strength analysis diagram of bottom rod of displacement sensor.

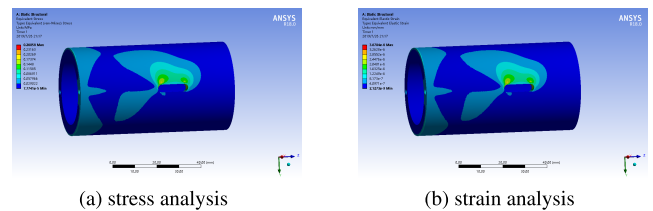


FIGURE 4. Strength analysis diagram of guide cylinder.

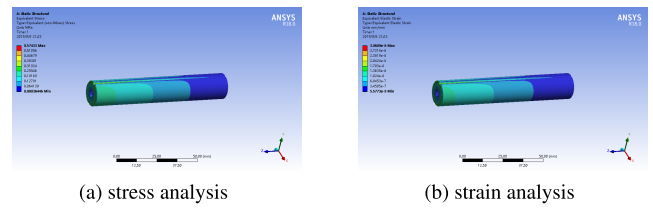


FIGURE 5. Strength analysis diagram of guide rod.

TABLE 2. Strength of key components of the compliant device.

The key components	Maximum stress (MPa)	Maximum strain (mm)
Top of the displacement sensor	3.399	1×10^{-3}
Bottom rod of displacement sensor	3.816	2.03×10^{-5}
Guide cylinder	0.216	3.67×10^{-6}
Guide rod	0.574	3.06×10^{-6}

III. PEG-IN-HOLE STRATEGY

A. ANALYSIS OF PEG-IN-HOLE PROCEDURE

FIGURE 6 shows the four states involved in the peg-in-hole assembly: contacting, searching, adjusting and inserting [24]. FIGURE 6(a) shows that the peg is in contact with the hole under a force that push the peg toward the hole. FIGURE 6(b) shows the hole searching process. In previous research, two main methods exist to find the hole:

(1) Spiral Search [25], [26]. Starting from the point where the peg contacts the outer surface of the hole, a constant pressure is maintained to make an outward spiral motion. As long as the pitch is small enough and the movement time is long enough, the peg will fall into the hole. However, this method will require a long time.

(2) Random Search [27]. This search is similar to the spiral search process, with the random movement of the peg in

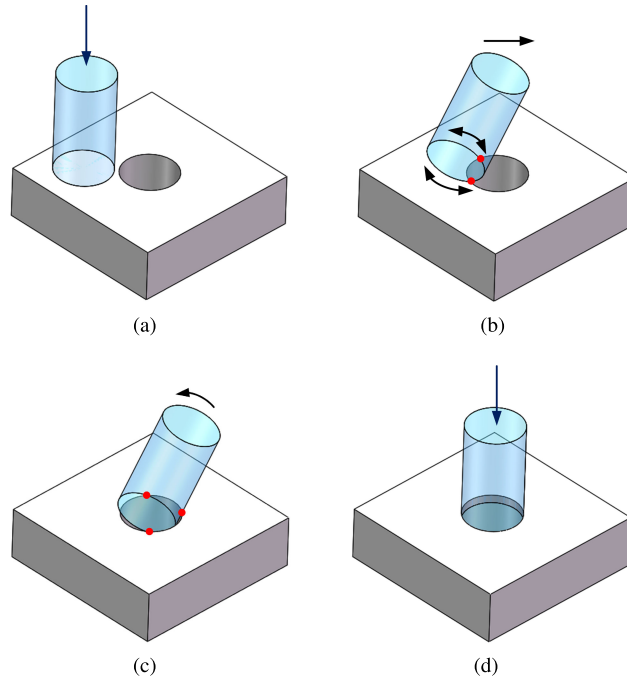


FIGURE 6. Peg-in-hole assembly process (a) Contacting (b) Searching (c) Adjusting (d) Inserting.

the plane of the outer surface of the hole, which reduces the average time of the search hole.

FIGURE 6(c) shows the pose adjustment process after the hole is located. Two main methods exist:

(1) Mechanical analysis [28]. After the peg was in contact with the hole, the force/torque sensor was used to obtain the value and direction of the contact force/torque. The geometric relationship between the peg and hole was used to establish a balance equation to solve the deflection direction of the peg. The corresponding posture adjustment of the peg was performed. However, detection of the states of the peg and hole contact is difficult.

(2) Sensorless posture adjustment. Representative was the concept of attraction region in environment proposed by Qiao *et al.* [29]. She assimilated the attraction region to the bottom of the bowl. There was a “bowl” in the high-dimensional operation space of the robot. The robot can accurately finish the assembly task by controlling the contact point from a rough position without using sensors.

Finally, the peg will fall into the hole when the tiling angle becomes zero, as shown in FIGURE 6(d).

In this paper, by using the proposed elastic displacement device, the search method in the proposed assembly strategy, which only needs to combine the elastic displacement device and the Cartesian coordinate system position control of the robot, is simplified. The searching task can be rapidly completed without chamfering and the error range is within the diameter of the peg. In this method, the peg can be inserted into the hole without complicated pose adjustment.

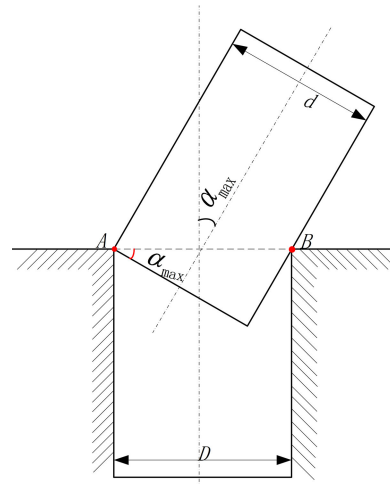


FIGURE 7. Two-point contact state when the inclination angle α is the maximum.

B. PEG-IN-HOLE STRATEGY

In the contact stage, to improve the success rate of the hole search and to simplify the pose adjustment process, the peg needs to be tilted by the small angle α , and the value of α is determined by the following methods.

(1) Maximum inclination of α .

When the inclination angle α is the maximum, the state of the most suitable two-point contact is shown in FIGURE 7, where d is the diameter of the peg, and D is the diameter of the hole. The maximum of angle α is the angle of declination of the peg’s axis relative to the axis of the hole where the jamming occurs.

The maximum of angle α is expressed by the parameters of the hole and the peg by the following expression:

$$\begin{cases} \cos\alpha_{max} = \frac{d}{D} \\ \alpha_{max} = \arccos\frac{d}{D} \end{cases} \quad (1)$$

If the inclination angle α continues to increase, the three-point contact state will appear, as shown in FIGURE 8(a). When the value of the inclination angle α decreases to 0, the contact state is shown in FIGURE 8(b). In this state, if the downward force is small, the peg will remain at the outer edge of the hole. If a large force is applied, the assembled parts may be damaged. Therefore, a series of complicated adjustments must be performed to make the peg fall into the hole. These adjustments will undoubtedly increase the difficulty and time of assembly. In the search stage, the angle should be less than the maximum of angle α .

(2) Minimum inclination of α .

When the inclination angle α is the minimum, the state of the three-point contact is the state shown in FIGURE 9, where D is the diameter of the hole, d is the diameter of the peg, and h is the depth of its insertion.

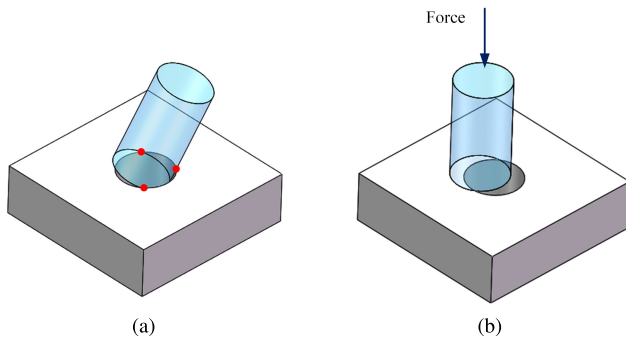


FIGURE 8. (a) Three-point contact state and (b) posture after adjustment is completed.

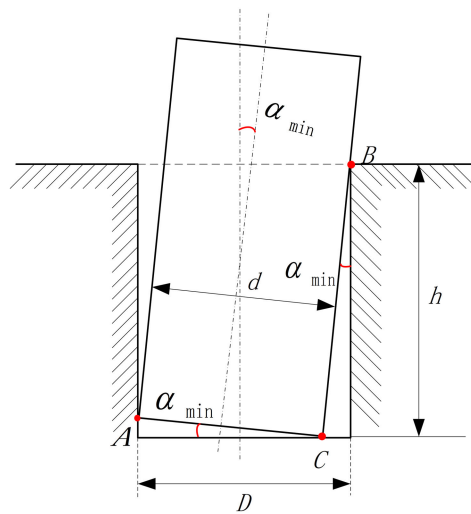


FIGURE 9. Three-point contact state when the inclination angle α is the minimum.

The minimum inclination of α as a function of the peg's depth of insertion into the hole is expressed by the following scheme:

$$D = d \cos \alpha_{min} + h \tan \alpha_{min} \quad (2)$$

If the inclination angle α continues decreasing, it will cause surface contact between the peg and the outer surface of the hole during the searching stage, which will be detrimental to the searching method in this paper. Surface contact may lead to the failure of the hole search. Therefore, the range of values of α should satisfy the (3):

$$\alpha_{min} \leq \alpha \leq \alpha_{max} \quad (3)$$

In the hole search stage, a strategy of rotating the assembly peg around the axis Z is employed.

The assembly peg is compressed along the axis to the maximum displacement, and the center position of the bottom surface of the peg is set to the position of the robot TCP. Which is also the compliant center of the assembly peg. As shown in FIGURE 10(a), the center point of the bottom surface of the peg is O_1 , and the center point of the upper surface of the hole is O_2 . The bottom surface of the peg is in

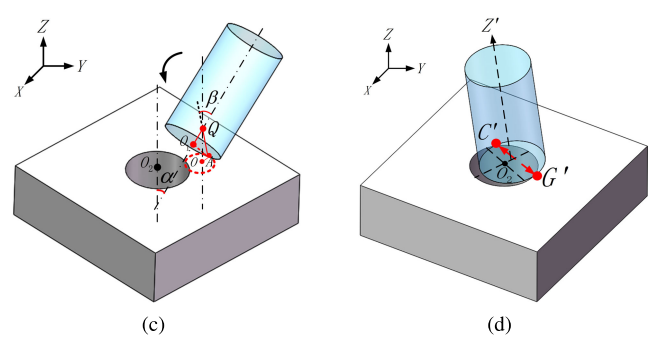
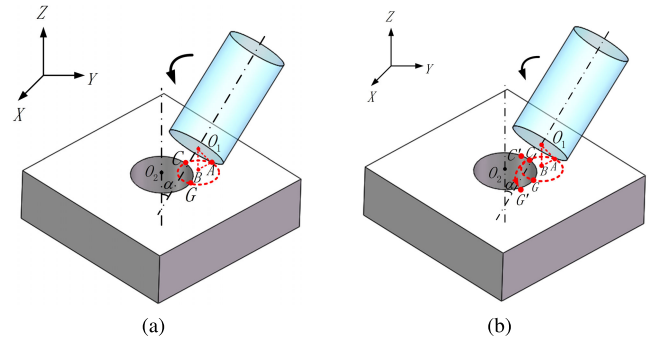


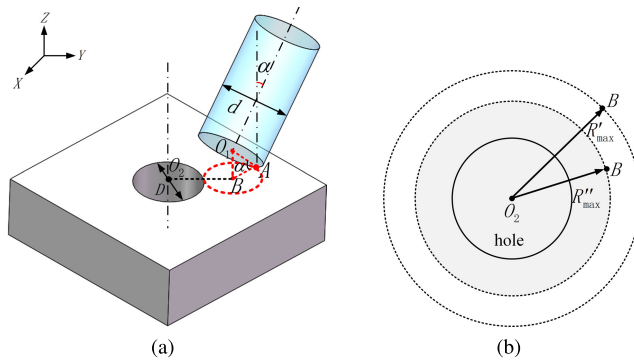
FIGURE 10. Hole searching process: The Y-axis is parallel to the upper surface of the hole and Y-axis of the robot base coordinate system, the Z-axis is parallel to the hole axis, and the X-axis is perpendicular to the Y-axis and Z-axis.

contact with the outer surface of the hole, and the projection of O_1 on the outer surface of the hole is B. The Z' axis of the assembly peg maintains the angle α and rotates around the Z axis.

If the peg is rigidly connected to the end of the robot, the compliant center O_1 position will remain unchanged when the peg rotates around the Z axis. The trajectory of the plane contact point between the peg and the outer surface of the hole is a circle with the center B and the radius AB. This trajectory intersects the outer edge of the hole at points C and G. In the arc CG segment, the peg and hole do not contact.

However, the upper end of the peg is connected to the elastic displacement device in this paper. The compliant center O_1 remains unchanged in the arc AC segment as shown in FIGURE 10(b). However, the assembly peg will be displaced along the Z' axis of the assembly peg due to the force of the spring after the point C. In addition, the position of the compliant center changes at the assembly peg. In the hole searching process, the contact point of the peg and hole gradually move from point C to point C' , and the contact state of the peg and the hole is always in a one-point contact state before contact with point G' . Line segment CG' is the trajectory of the lowest point of the lower surface of the peg. When in contact with point G' , the peg will be displaced in the opposite direction along the Z' axis.

When the compliant center moves along the axis of the assembly axis to the point Q, as shown in FIGURE 10(c),

**FIGURE 11.** Position deviation of the peg and hole.

the Q point is projected as point O on the outer surface of the hole. The trajectory of the contact point between the peg and the outer surface of the hole is a circle with radius OA . The angle between line segment QA and the axis of the assembly peg is β , and line segment O_1Q is the displacement of the compliance center; its value is L , as measured by the displacement sensor. The values of OA should satisfy (4):

$$\begin{cases} R_{OA} = \sqrt{L^2 + d^2} \sin(\beta - \alpha) \\ \beta = \arctan \frac{d}{2L} \end{cases} \quad (4)$$

Assume that the assembly peg moves upward in the positive direction and downward in the negative direction and that displacements in different directions will inevitably occur at points C and G' . At this time, the peg has two-point contact with the outer edge of the hole, as shown in FIGURE 10(d). The geometric relationship reveals that the position of the hole center is on the vertical line of line $C'G'$ and the projection of the Z' axis of the assembly peg on the O-XY plane.

To ensure that the position of the hole can be located when the peg rotates around the Z axis. The deviation O_2B of the peg and hole must be smaller than the maximum deviation as shown in FIGURE 11(a).

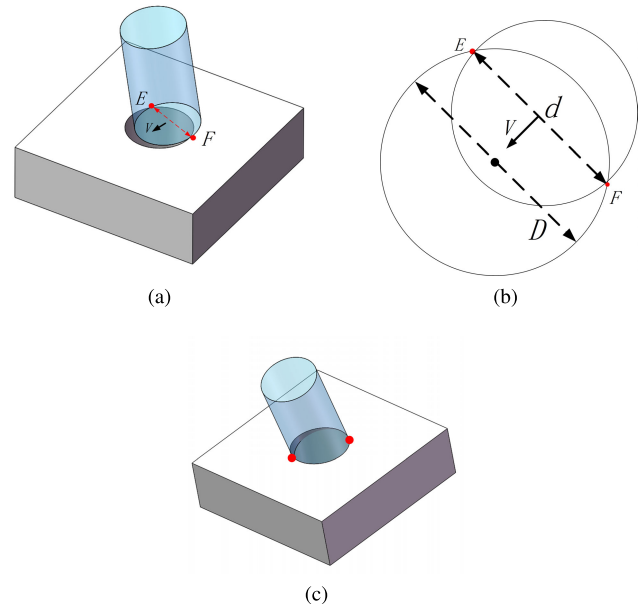
The deviation of the peg and hole is expressed as (5).

$$R' < \frac{D}{2} + \frac{d}{2} \cos \alpha \quad (5)$$

where R' is the value of the deviation O_2B of the peg and hole. Substituting (3) and after transformation, the range of positional deviations of the peg and hole will have the following expression:

$$\begin{cases} R'_{max} = \frac{D}{2} + \frac{d}{2} \cos \alpha_{min} \\ R''_{max} = \frac{D}{2} + \frac{d}{2} \cos \alpha_{max} \end{cases} \quad (6)$$

When the value of deviation R' of the peg and hole is equal to R''_{max} , the angle of inclination α can be adjusted between α_{min} and α_{max} , and the optimum peg and hole deviation, as shown in the gray area of FIGURE 11(b), ranges between 0 and R''_{max} .

**FIGURE 12.** Process of moving the assembly peg toward the center of assembly hole.

The stage of posture adjustment has two steps:

1) POSITION ADJUSTMENT OF THE ASSEMBLY PEG

The assembly peg should be moved in the oblique direction, at speed V during time t . In the searching stage, the angle at which the peg rotates around the Z axis is θ . At the end of the searching, the coordinates of the compliant center in the O-XY plane are (X_o, Y_o) . The direction in which the peg moves is expressed as follows:

$$\begin{cases} X = X_o + Vt \cos \theta \\ Y = Y_o + Vt \sin \theta \end{cases} \quad (7)$$

In the process of moving the peg toward the hole, as shown in FIGURE 12(a), since the diameter of the hole is larger than the diameter of the peg, the line-segment EF at the edge of the hole has the same diameter as the peg and is perpendicular to the moving direction, as shown in Figure 12(b). If the peg is rigidly connected to the robot, the assembly peg will not contact the hole during the moving process through the line-segment EF . However, the elastic displacement device in this paper will generate elastic force. At this time, the displacement of the peg will suddenly change under the effect of the elastic force, and the peg will enter the contact state of FIGURE 12(c).

2) POSTURE ADJUSTMENT OF THE ASSEMBLY PEG

The peg is rotated around the compliant center in a direction in which the inclination angle α decreases when the posture is adjusted. When the inclination angle of the assembly peg is $\alpha_{min} \leq \alpha_o \leq \alpha_{max}$, the position of the compliant center is shown in FIGURE 13:

In FIGURE 13(a), the blue and red lines represent the contact states of the peg with the left inner hole and right

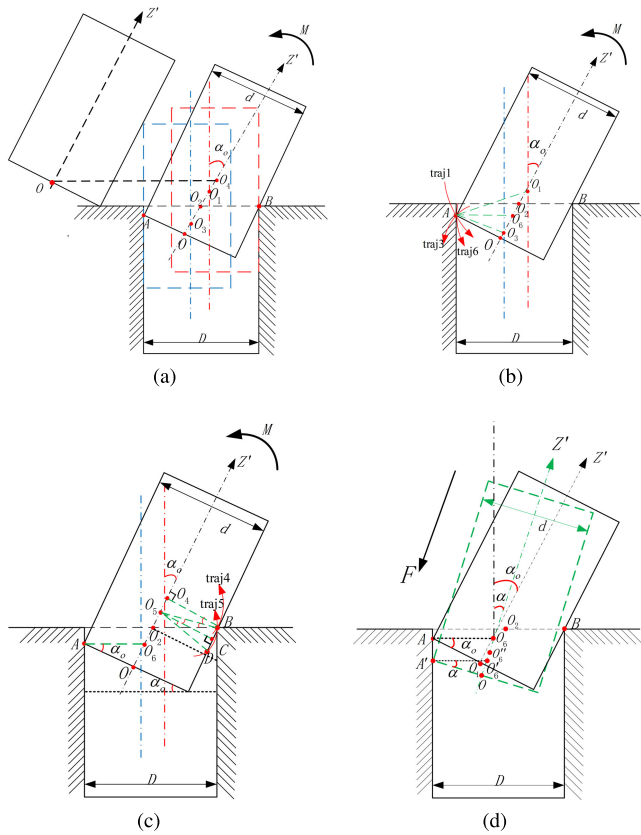


FIGURE 13. Posture adjustment based on variable compliance center.

inner hole, respectively, when the adjustment is completed. The intersection of the Z' axis of the peg after adjustment and the Z' axis of the peg before adjustment are points O_1 and O_3 . Correspondingly, point O_2 is the intersection of the plane where the outer surface of the hole is located and the Z' axis of the peg before adjustment. Point O_4 is the position of the initial compliant center after radial movement. Points A and B are the points at which the peg and the hole are in contact.

$$OO_4 = \frac{D - d\cos\alpha_o}{\sin\alpha_o} \quad (8)$$

As shown in FIGURE 13(b), $AO_6//BO_2$, which is the assembly peg for posture adjustment. When the compliant center is at O_3 , the trajectory of the contact point A is $traj3$, and the inner wall of the hole interferes with each other, which will cause the peg to be stuck. When the compliant center is at O_6 , the trajectory of the contact point A is $traj6$, which is tangent to the inner wall of the hole. When the compliant center is at O_1 , the trajectory of the contact point A is $traj1$, which moves in the direction of the separated contact. When the compliance center is above O_6 , the contact point A does not interfere with the assembly hole.

As shown in FIGURE 13(c), $O_4B \perp OO_4$, $\angle O_4BO_2 = \alpha_o$, $O_5C \perp OO_4$, $O_5B = O_5D$, and $\angle O_4BO_5 = \angle O_5BO_2 = \angle BO_5C = \angle DO_5C$. If the assembly peg is rigidly connected to the robot, when the compliance center is at O_4 , the trajectory of the contact point B is $traj4$,

which interferes with the assembly peg and causes the peg to be stuck. When the compliant center is at O_5 , the trajectory of the contact point B is $traj5$, and the intersection with the assembly axis is point B and point D . At BC of the assembly peg, it is separated from the assembly hole as α is reduced and is close to the assembly hole as α decreases at CD of the assembly peg. Since O_5B is the angle bisector of $\angle O_4BO_2$, when $\alpha = 0$, point D moves to point B . Therefore, when the compliance center is at O_5 , the contact point B does not interfere with the assembly peg. The assembly process is similar to the previous process when it is connected to the robot by the elastic displacement device.

When the compliant center is between O_5 and O_6 , the assembly peg does not interfere with the assembly hole.

To reduce the torque on the compliant center generated by the friction between the peg and hole during the posture adjustment, we set the position of the compliant center to O_6 at the end of the radial movement of the assembly peg. The distance of the compliance center that moves along the Z' axis is O_4O_6 .

$$O_4O_6 = \frac{D - d\cos\alpha_o}{\sin\alpha_o} - \frac{d}{2}\tan\alpha_o \quad (9)$$

The posture adjustment process is shown in FIGURE 13(d), $A'O'_6//AO_6$, $O_1O_6 = OO''_6$, $O_6O''_6 = \Delta L$, $AO_6 > \frac{d}{2}$, and $A'O'_6 > \frac{d}{2}$. As the tilt angle α decreases, the assembly peg always maintains one-point contact with the inside of the assembly hole under the elastic force of the compliant device. The contact point changes from the initial point A to A' , and the contact point B gradually separates from the inner wall of the hole. The compliant center changes from O_6 to O'_6 and is always between the axis of blue and the axis of red in FIGURE 13(a). ΔL is the displacement value of the assembly peg measured by the displacement sensor. The process of changing the compliant center along the negative direction of the Z' axis is shown in (10).

$$\Delta Z' = \frac{d}{2}(\tan\alpha_o - \tan\alpha) + \Delta L \quad (10)$$

IV. CONTROL FRAMEWORKS

During the interaction between the robot end effector and the target, due to the large rigidity of the external environment, a small deformation will generate a large contact force, which may damage the workpiece and the robot. This paper introduces an elastic compliant device in section II that directly controls the position of the robot via the generated displacement signal generated by it, which renders the control process easier and more convenient. The block diagram of the assembly control system is shown in FIGURE 14.

In assembly tasks, past information is indispensable if a robot controller is to understand the current situation. For example, the robot cannot distinguish jamming from a normal insertion with large displacement. To solve this problem, we design a position controller according to the assembly process. The position controller obtains the state $S(t)$ of the assembly system and generates the control signal according

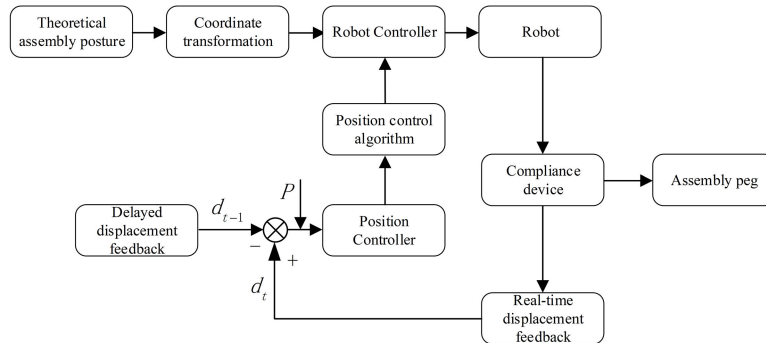


FIGURE 14. Block diagram of the assembly control system.

to this state. The robot controller executes motion planning by the position control algorithm. The current information is obtained by real-time displacement feedback of the compliant device, and past information is obtained by setting the delay time t . The definition of $S(t)$ is provided in (11):

$$S(t) = (\Delta d, P) \quad (11)$$

where $\Delta d = d_t - d_{t-1}$ and $P = \frac{\text{insert displacement}}{\text{depth}_{\text{hole}}}$ are the change in displacement and the extent of insertion of the assembly peg, which are used to guide the assembly process and infer if the peg is jammed. In the hole searching stage, when $\Delta d < 0$, the assembly peg and hole is in a one-point contact state. Correspondingly, $\Delta d > 0$ represents a two-point contact state. In the position adjustment stage, $\Delta d = 0$ means the position adjustment is completed. In the insertion stage, $\Delta d = 0$ and $P = 1$ represent that the assembly peg is completely pushed into the hole bottom, which is considered a success of the assembly. To avoid robot and workpiece damage. The Δd and P should be limited:

$$\begin{cases} \Delta d^{\text{limited}} < \varepsilon \rightarrow 0^+ \\ \Delta d^{\text{limited}} > \varepsilon \rightarrow 0^- \\ 0 \leq P \leq 1 \end{cases} \quad (12)$$

In theory, the value of ε should be 0 in the hole search stage. Since the peg has the tilt angle α , the elastic force of the compliant device may cause the assembly peg and hole to slide relative to each other. In addition, changes in the compliant center will also cause relative displacement of the peg and hole. Therefore, the value of ε will be greater than 0 or less than 0. We will perform experiments to explore the relations between ε and the assembly rate of success, and then determine the delay time t .

In FIGURE 15, the measured values of the assembly success rate are indicated with a dot. The relations between $f(\varepsilon)$ and the assembly success rate $f(\varepsilon)$ were estimated using Gaussian curve fitting, as expressed by (13).

$$f(\varepsilon) = a \exp \left[- \left(\frac{\varepsilon - b}{c} \right)^2 \right] \quad (13)$$

According to the estimation results, a , b , and c in (12) are set to 0.973, 0.082 and 0.075, respectively. This equation

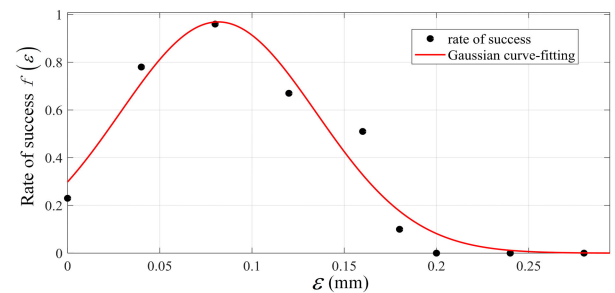
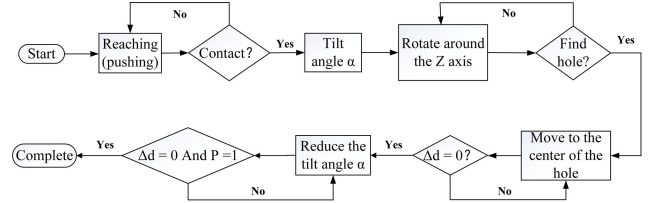
FIGURE 15. Gaussian curve-fitting graph of the relations between ε and assembly rate of success $f(\varepsilon)$.

FIGURE 16. Peg-in-hole assembly process.

theoretically verifies the maximal values of the assembly success rate $f(\varepsilon)$ when $b = \varepsilon$. To determine a suitable delay time t is 10 ms. The complete peg-in-hole assembly process is shown in FIGURE 16.

V. THEORETICAL ERROR ANALYSIS

The errors in the assembly strategy of a peg-in-hole assembly with variable compliance centers is mainly caused by the delay of the system response. The errors mainly occur in the searching holes and adjusting position process. The magnitude of errors is mainly related to the angular velocity of searching holes and the radial velocity of moving towards holes in the adjusting position. The smaller the values of angular velocity and radial velocity are, the smaller the error is, and the longer the assembly time is. Conversely, the errors will be larger, which may cause assembly failure.

The maximum error caused by the searching hole is expressed as follows:

$$e_f = \frac{d}{2} \omega t_0 \quad (14)$$

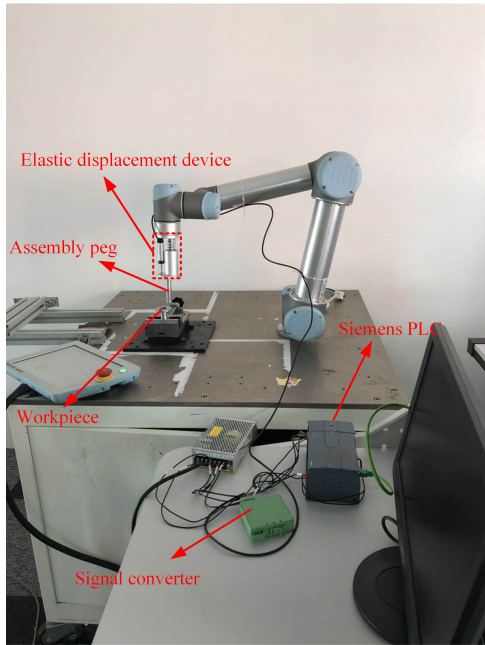


FIGURE 17. Experimental environment of peg-in-hole assembly.

The maximum error caused by radial movement to the hole is expressed as follows:

$$e_r = vt_0 \quad (15)$$

Thus, the maximum deviation after adjusting the peg and hole is expressed as:

$$e_{max} = \sqrt{e_f^2 + e_r^2} \quad (16)$$

where t_0 is the delay time of the system, ω is the angular velocity of hole searching, and v is the radial velocity of moving towards hole in the adjusting position.

VI. EXPERIMENT

In order to verify the assembly method in this paper proposed, UR5 robot is selected and the end is connected with the elastic displacement device. The displacement sensor signal is collected and controlled by Siemens PLC and Intel(R) Core(TM) i7-6700 CPU computer. The peg is fixed at the end of the elastic displacement device, and the workpiece is fixed on the fixture. The experimental environment is shown in FIGURE 17.

The diameter of the peg is 15.97mm, the diameter of the hole is 16.07 mm, and the clearance between the peg and the hole is 0.1 mm. The delay time of the system is less than 30 ms. The movement speed of the robot in the peg and hole contact phase is 13 mm/s. The speed of movement to the center of the assembly hole is 8.5 mm/s. The rotation speed of the assembly peg around the Z axis is 20°/s, and no chamfers exist in the peg and hole. The assembly experimental process is shown in FIGURE 18.

The following parameter can be obtained from (1), (2), (6), (8) and (16). $\alpha_{max} = 6.4^\circ$, $\alpha_{min} = 0.4^\circ$, $0 < R' < 15.97\text{mm}$, $e_{max} = 0.28\text{mm}$, when $\alpha_o = 6^\circ$, $OO_4 = 1.79\text{mm}$.

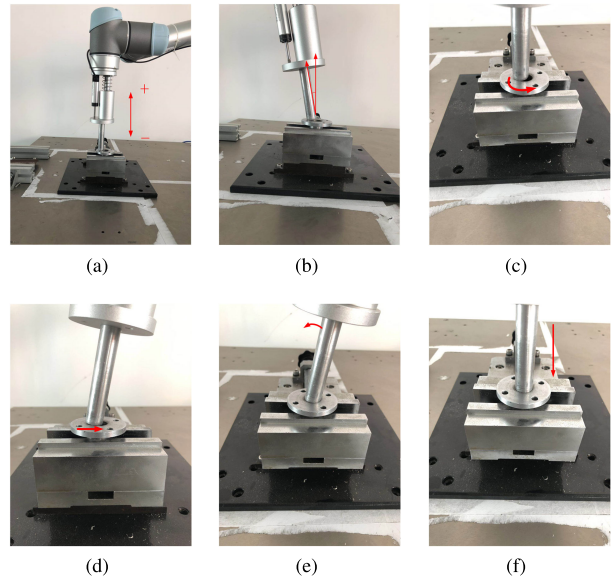


FIGURE 18. Procedure of the peg-in-hole assembly experiments.

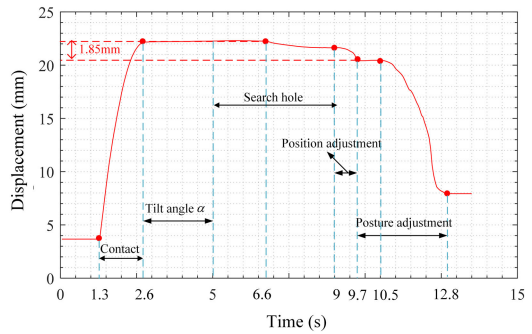


FIGURE 19. Distance between center of peg and hole is 5 mm, inclination angle α is 60° .

As shown in FIGURE 19, at 1.3s, the peg begins to contact the outer surface of the hole. At 2.6s, the peg compresses to the position of TCP set by the robot. From 2.6s to 5s, the assembly peg is tilted by the angle α around the Y axis. From 5s to 9s, the peg rotates around the Z axis on the outer surface of the hole. At 6.6s, the peg contacts the outer edge of the hole. After 6.6s, the peg is displaced by the elastic force of the elastic displacement device, and the displacement gradually decreases. At 9s, the displacement inversely increases. At this time, two points contact the outer edge of the hole. The peg moves along the radial direction of the hole in 9 – 9.7s, and its displacement abruptly changes in 9.5s. The inclination angle of the peg gradually decreases in 9.7 – 13s. However, at 9.7 – 10.5s, the displacement of the assembly peg undergoes minimal change because the frictional force between the peg and the hole are greater than the component of the elastic force of the compliant device in the vertical direction. At 10.5 – 13s, the friction force decreases with a decrease in α , and the peg is inserted in the hole under the action of elasticity. At this time, the robot completes the assembly task.

In addition, at 6.6s–9.7s, the displacement of the peg under the elastic force of elastic displacement device is 1.85mm

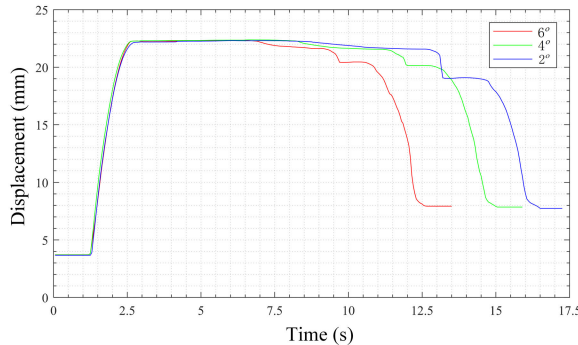


FIGURE 20. Distance between center of peg and hole is 5 mm, and inclination angle α is 6° , 4° , and 2° , respectively.

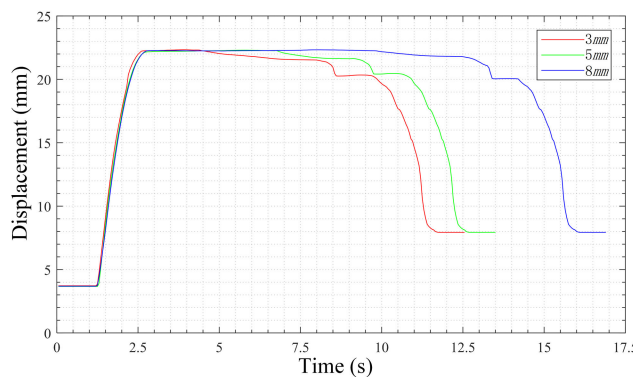


FIGURE 21. Inclination angle α is 6° , and distance between center of peg and hole is 3mm, 5mm, and 8mm, respectively.

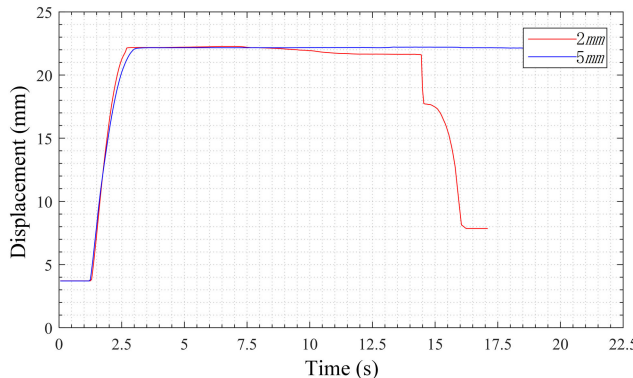


FIGURE 22. Inclination angle α is 1.3° , and distance between center of peg and hole is 2mm and 5mm, respectively.

when $\alpha = 6^\circ$. The theoretical displacement is 1.79mm, which further verifies the correctness of the proposed method.

As shown in FIGURE 20, the larger the inclination angle α is when it is in the range of (3), the faster the hole searches, and the less time is required it takes to complete the assembly task. As shown in FIGURE 21, the shorter the R' becomes between the center of the peg and the hole, the faster the hole searches, and the less time is required to complete the assembly task.

As shown in FIGURE 22, the searching hole fails when the inclination angle α of the assembly peg is 1.3° , and the distance between the peg and the hole center is 5mm. However, when the distance R' between the axis and the hole center

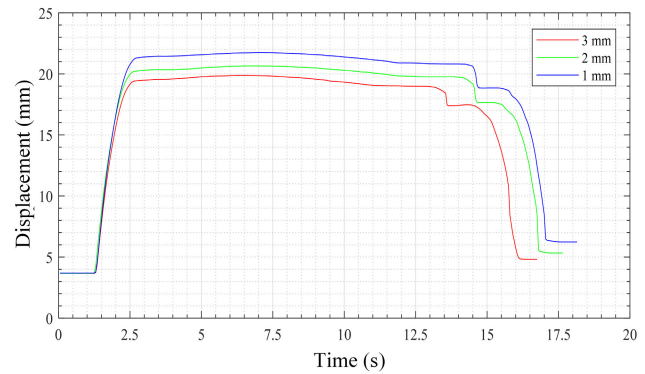


FIGURE 23. The distance between center of peg and hole is 5 mm, and inclination angle α is 6° . The distance between the compliant center position and the bottom center of the peg is 3mm, 2mm, and 1mm.

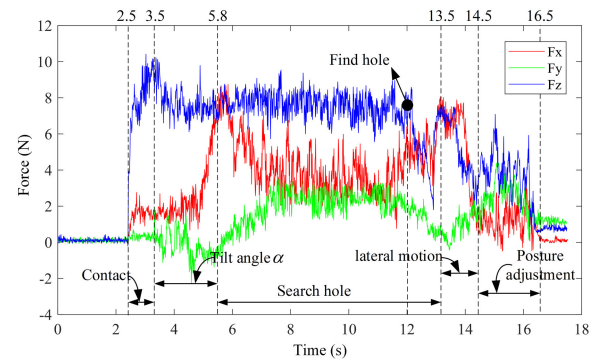


FIGURE 24. Change process of contact force during peg-in-hole assembly.

is 2mm, the assembly is successful. Thus, the forecasting of the hole searching stage analysis is validated. In addition, if we assume that $\alpha_{max} = 1.3^\circ$ and $D = 16.07\text{mm}$, then $d = D \cos \alpha_{max} = 16.066\text{mm}$. The clearance between the peg and the hole is 0.004mm. In theory, the precision of the assembly method in this paper is 0.004mm.

FIGURE 23 shows that the assembly efficiency can be improved by properly increasing the position of the compliant center.

In theory, the error analysis of the assembly shows that the maximum error $e_{max} = 0.28\text{mm}$, which is larger than the clearance between the peg and the hole (0.1 mm). However, the assembly is successful. After observation, the collision with the hole occurs at the end of the radial movement of the peg. Therefore, in the actual assembly tasks, the speed of radial movement should be reduced as much as possible.

As shown in FIGURE 24, from 2.5s – 3.5s, the assembly peg is in contact with the hole, the spring of the compliant device is compressed and the F_z is gradually increased. From 3.5s – 5.8s, the assembly peg is tilted by the angle α around the Y axis, and the F_x , F_y , and F_z fluctuate due to a slight slippage of the assembly peg and the hole. However, F_x gradually increases as the angle α increases. In this process, F_y does not substantially change. From 5.8s – 13.5s, the hole search process is performed, and the position of the hole is found at 12s. At this time, the peg and hole is in a one-point contact

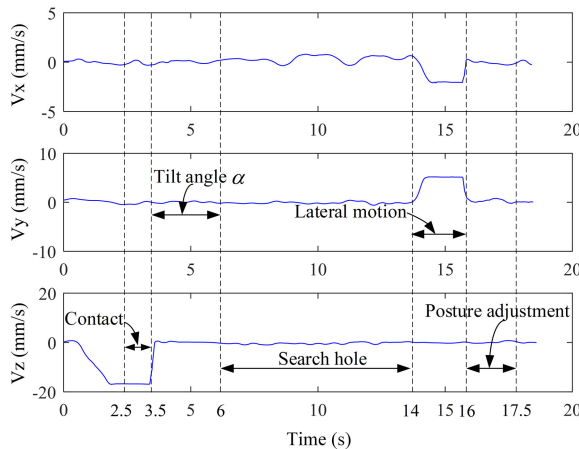


FIGURE 25. Velocity change process of assembly peg during peg-in-hole assembly.

state. At $13.5s$, the hole is searched, and the peg and hole are in a two-point contact state, as shown in FIGURE 12(a). From $13.5s - 14.5s$, the assembly peg moves toward the center of the assembly hole, and F_x , F_z gradually decrease. The inclination angle α of the assembly peg is gradually reduced from $14.5s - 16.5s$, the assembly peg is inserted into the assembly hole under the action of the elastic force, and the contact force is gradually reduced.

As shown in FIGURE 25, From $0 - 2.5s$, V_z gradually increases to the set assembly speed. From $2.5s - 3.5s$, the assembly peg comes into contact with the assembly hole. At $3.5s$, the center of the bottom of the assembly peg coincides with the TCP of the robot. At the same time, the robot receives the displacement signal of the compliant device and stops moving. Thus, the V_z is abruptly changed to 0. From $3.5s - 14s$ and $16s - 17.5s$, since the TCP position of the robot does not change, V_x , V_y , and V_z are 0. From $14s - 16s$, during the lateral movement of the assembly peg, V_x and V_y attain reach the set lateral movement speed. At $16s$, the robot obtains the signal of the end of the lateral movement and stops moving, and V_x and V_y becomes 0. At $17.5s$, the peg-in-hole assembly is completed.

VII. PERFORMANCE COMPARISONS

In general, robots should apply some assembly strategies of compliance when they make contact with external environments. Therefore, the hole search strategy in section III and the strategy proposed in this paper are compared and analyzed.

(1) Spiral search. The spiral search is a commonly employed method in peg-in-hole assembly tasks. The point contacted by the peg and hole is the starting point of the search. The workpiece makes an Archimedes spiral motion outward on the X-Y plane. In polar coordinates, the Archimedes spiral trajectory is defined by [24].

$$\begin{cases} \delta\theta = \frac{d}{r_i} \\ r_{i+1} = r_i + \delta\theta \frac{c}{2\pi} \end{cases} \quad (17)$$

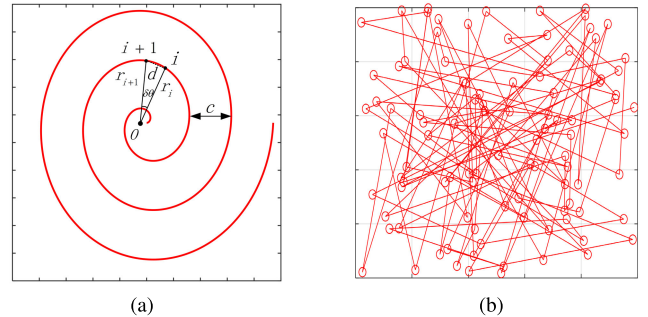


FIGURE 26. (a) Spiral search trajectory (b) Random search waypoints and trajectory (c) Search trajectory in this paper.

where d denotes the distance between the current position and previous position. c is the pitch of the Archimedes spiral, as shown in FIGURE 26(a), while ensuring that the hole is on the search path. The search region is experimentally determined to be 2σ , where σ is the maximum positional error.

(2) Random search. The random search is the simpler method in the search strategy. In a random search, the peg is moved in random directions throughout the search region on the X-Y plane. In Cartesian coordinates, this movement is described as [25].

$$\begin{cases} x_{i+1} = x_i + (K_x * rand()) \\ y_{i+1} = y_i + (K_y * rand()) \end{cases} \quad (18)$$

where $rand()$ is a function that can generate a random value in the range $[-2\sigma, 2\sigma]$ and K_x, K_y are the search step gain for X and Y -axes, which is mainly related to the scope of the search region. The random search region is a square region with a side length of 2σ by experiment. The random search trajectory is shown in FIGURE 26(b).

(3) The search in this paper. The rotational motion of the assembly peg around the compliant center. The trajectory of the contact point between the lower surface of the inclined assembly peg and the hole is as shown in FIGURE 26(c). From the previous description of FIGURE 10(c), the definition of the hole search trajectory in polar coordinates can be

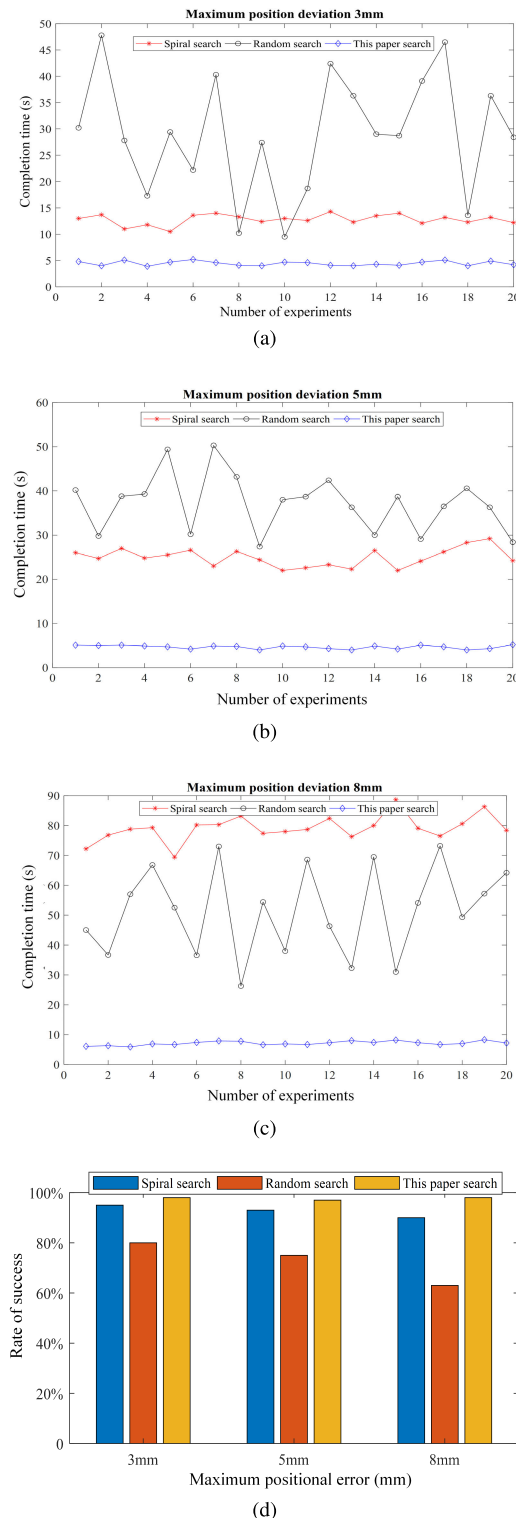


FIGURE 27. (a), (b), and (c) Completion Time (CT) of the maximum deviation is 3 mm, 5 mm, and 8 mm and (d) Rate of Success (RS) of different search methods with different position errors.

obtained, as shown in (19).

$$r = \begin{cases} \frac{d}{2} \cos\alpha, & (L = 0) \\ \sqrt{L^2 + d^2} \sin(\beta - \alpha), & (L > 0) \end{cases} \quad (19)$$

Two metrics were employed to measure the performance of the hole search in a robotic peg-in-hole assembly task [26].

(1) Completion Time(CT): The time to complete the hole search. From the time when the assembly peg contacts the outer surface of the hole to the time before the location of the hole is found and the next adjustment is performed, the period is CT. To improve the credibility, 20 experiments were separately performed with different maximum position deviations.

(2) Rate of Success(RS): The value of RS is determined by the number of samples and successes. Twenty comparative experiments will be conducted to calculate the success rate.

In this comparative experiment, the pitch c of the spiral search is $2e$ [30]; the peg and hole tolerance is e , and the interval between two adjacent way points is 8 ms. In the random search, the step gain must be small to avoid damage to the robots and workpieces [25]; thus, it is set to $K_x = K_y = 0.1$. The time interval is 8ms. The moving speed of the TCP terminal of the robot is 13mm/s. The maximum positional error is 3mm, 5mm, and 8mm. Since the peg and hole in this experiment are chamferless, to improve the efficiency of the hole search, the peg is inclined at an angle $\alpha = 6^\circ$. The performance comparison results are shown in FIGURE 27.

A comparison of the experimental results of the method of hole search in this paper with those of the common methods of hole search are shown in FIGURE 27. For different position deviations, the stability of the random hole searching method is poor. The spiral search hole and the method of this paper have higher stability. As the position deviation increases, the time for spiral hole search significantly increases. So the search method in this paper is very stable and superior with regard to the completion time. Compared with the random search, the RS is distinctly obviously improved.

VIII. CONCLUSION

In this paper, a new peg-in-hole assembly strategy is proposed, and an elastic displacement device is designed based on this strategy. This method combines the advantages of active compliance and passive compliance, and does not require any type of force/torque sensors. The control system is relatively simple. First, the structure and performance of the elastic displacement device are introduced, and the contact state of the peg and hole is analyzed based on the elastic displacement device. The validity of this method is verified by experiments and has a higher assembly efficiency. The experiments show that the method proposed in this paper can successfully complete the peg-in-hole assembly task when tilt and position deviation occur in the assembly peg and hole. The search method in this paper is superior with regard to the completion time. Although the strategy presented in this paper has successfully realized a precision peg-in-hole assembly, only a single round peg-in-hole assembly is currently available. We are working hard to improve

the assembly strategy described in this paper to apply it to multiple peg-in-hole and complex shape assembly tasks.

IX. ACKNOWLEDGMENT

(Sen Wang and Guodong Chen are co-first authors.)

REFERENCES

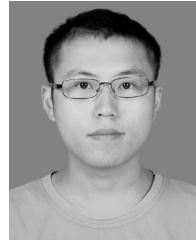
- [1] J. L. Nevins and D. E. Whitney, *Concurrent Design of Products and Processes: A Strategy for the Next Generation in Manufacturing*. New York, NY, USA: McGraw-Hill, 1989.
- [2] F. Zhao and P. S. Y. Wu, “VRCC: A variable remote center compliance device,” *Mechatronics*, vol. 8, no. 6, pp. 657–672, 1998.
- [3] S. Lee, “Development of a new variable remote center compliance (VRCC) with modified elastomer shear pad (ESP) for robot assembly,” *IEEE Trans. Autom. Sci. Eng.*, vol. 2, no. 2, pp. 193–197, Apr. 2005.
- [4] D. I. Park, H. Kim, C. Park, T. Choi, H. Do, B. Kim, and J. Park, “Automatic assembly method with the passive compliant device,” in *Proc. 11th Asian Control Conf. (ASCC)*, Dec. 2017, pp. 347–348.
- [5] N. Hogan, “Impedance control: An approach to manipulation,” in *Proc. Amer. Control Conf.*, Jun. 1984, pp. 304–313.
- [6] Y. Li, S. S. Ge, Q. Zhang, and T. H. Lee, “Neural networks impedance control of robots interacting with environments,” *IET Control Theory Appl.*, vol. 7, no. 11, pp. 1509–1519, 2013.
- [7] J. Krüger, G. Schreck, and D. Surdilovic, “Dual arm robot for flexible and cooperative assembly,” *CIRP Ann.*, vol. 60, no. 1, pp. 5–8, 2011.
- [8] L. Roveda, F. Vicentini, N. Pedrocchi, and L. M. Tosatti, “Force-tracking impedance control for manipulators mounted on compliant bases,” in *Proc. IEEE Int. Conf. Robot. Autom. (ICRA)*, May/Jun. 2014, pp. 760–765.
- [9] L. Roveda, N. Iannacci, F. Vicentini, N. Pedrocchi, F. Braghin, and L. M. Tosatti, “Optimal impedance force-tracking control design with impact formulation for interaction tasks,” *IEEE Robot. Autom. Lett.*, vol. 1, no. 1, pp. 130–136, Jan. 2015.
- [10] A. Flores-Abad, A. Crain, M. Nandayapa, M. A. Garcia-Teran, and S. Ulrich, “Disturbance observer-based impedance control for a compliance capture of an object in space,” in *Proc. AIAA Guid., Navigat., Control Conf.*, 2018, p. 1329.
- [11] F. Zeng, J. Xiao, and H. Liu, “Force/torque sensorless compliant control strategy for assembly tasks using a 6-DOF collaborative robot,” *IEEE Access*, vol. 7, pp. 108795–108805, 2019.
- [12] M. H. Raibert and J. J. Craig, “Hybrid position/force control of manipulators,” *J. Dyn. Syst., Meas., Control*, vol. 103, no. 2, pp. 126–133, 1981.
- [13] D. J. Giblin, Y. Liu, and K. Kazerounian, “Target tracking robotic manipulation theories applied to force/position control in peg-in-hole assembly tasks,” *Int. J. Robot. Autom.*, vol. 23, no. 1, p. 49, 2008.
- [14] Q. Fang, W. Chen, A. Zhao, C. Deng, and S. Fei, “Control system designing for correcting wing-fuselage assembly deformation of a large aircraft,” *Assembly Autom.*, vol. 37, no. 1, pp. 22–33, 2017.
- [15] L. Ma, W. Rong, and L. Sun, “Multi-sensor control for precise assembly of optical components,” *Chin. J. Aeronaut.*, vol. 27, no. 3, pp. 613–621, 2014.
- [16] S. Chiaverini and L. Sciavicco, “Force/position control of manipulators in task space with dominance in force,” *IFAC Proc. Vol.*, vol. 21, no. 16, pp. 137–143, 1988.
- [17] S. Flixeder, T. Glück, and A. Kugi, “Modeling and force control for the collaborative manipulation of deformable strip-like materials,” *IFAC-PapersOnLine*, vol. 49, no. 21, pp. 95–102, 2016.
- [18] C.-C. Chen, J.-S. Li, J. Luo, S.-R. Xie, H.-Y. Li, H.-Y. Pu, and J. Gu, “Robust adaptive position and force tracking control strategy for door-opening behaviour,” *Int. J. Simul. Model.*, vol. 15, no. 3, pp. 423–435, 2016.
- [19] Z. Jakovljevic, P. B. Petrovic, V. D. Mikovic, and M. Pajic, “Fuzzy inference mechanism for recognition of contact states in intelligent robotic assembly,” *J. Intell. Manuf.*, vol. 25, no. 3, pp. 571–587, 2014.
- [20] T. Inoue, G. De Magistris, A. Munawar, T. Yokoya, and R. Tachibana, “Deep reinforcement learning for high precision assembly tasks,” in *Proc. IEEE/RSJ Int. Conf. Intell. Robots Syst. (IROS)*, Sep. 2017, pp. 819–825.
- [21] J. Xu, Z. Hou, W. Wang, B. Xu, K. Zhang, and K. Chen, “Feedback deep deterministic policy gradient with fuzzy reward for robotic multiple peg-in-hole assembly tasks,” *IEEE Trans. Ind. Informat.*, vol. 15, no. 3, pp. 1658–1667, Jul. 2019.
- [22] Y. Fan, J. Luo, and M. Tomizuka, “A learning framework for high precision industrial assembly,” in *Proc. Int. Conf. Robot. Autom. (ICRA)*, May 2019, pp. 811–817.
- [23] M. A. Lee, Y. Zhu, K. Srinivasan, P. Shah, S. Savarese, L. Fei-Fei, A. Garg, and J. Bohg, “Making sense of vision and touch: Self-supervised learning of multimodal representations for contact-rich tasks,” in *Proc. Int. Conf. Robot. Autom. (ICRA)*, May 2019, pp. 8943–8950.
- [24] H. Park, J. Park, D.-H. Lee, J.-H. Park, M.-H. Baeg, and J.-H. Bae, “Compliance-based robotic peg-in-hole assembly strategy without force feedback,” *IEEE Trans. Ind. Electron.*, vol. 64, no. 8, pp. 6299–6309, Aug. 2017.
- [25] J. A. Marvel, R. Bostelman, and J. Falco, “Multi-robot assembly strategies and metrics,” *ACM Comput. Surv.*, vol. 51, no. 1, 2018, Art. no. 14.
- [26] K. Van Wyk, M. Culleton, J. Falco, and K. Kelly, “Comparative peg-in-hole testing of a force-based manipulation controlled robotic hand,” *IEEE Trans. Robot.*, vol. 34, no. 2, pp. 542–549, Apr. 2018.
- [27] M. A. Habib, M. S. Alam, and N. H. Siddique, “Optimizing coverage performance of multiple random path-planning robots,” *Paladyn*, vol. 3, no. 1, pp. 11–22, 2012.
- [28] Y. Xia, Y. Yin, and Z. Chen, “Dynamic analysis for peg-in-hole assembly with contact deformation,” *Int. J. Adv. Manuf. Technol.*, vol. 30, nos. 1–2, pp. 118–128, 2006.
- [29] H. Qiao, M. Wang, J. Su, S. Jia, and R. Li, “The concept of ‘attractive region in environment’ and its application in high-precision tasks with low-precision systems,” *IEEE/ASME Trans. Mechatronics*, vol. 20, no. 5, pp. 2311–2327, Oct. 2015.
- [30] S. R. Chhatpar and M. S. Branicky, “Search strategies for peg-in-hole assemblies with position uncertainty,” in *Proc. IEEE/RSJ Int. Conf. Intell. Robots Syst. Expanding Soc. Role Robot. Next Millennium*, vol. 3, Oct./Nov. 2001, pp. 1465–1470.



SEN WANG was born in 1992. He received the B.E. degree from Ningbo University, Ningbo, China, in 2017. He is currently pursuing the M.S. degree with the School of Mechanical and Electric Engineering, Soochow University. His research interests include robot vision, force/position control, and compliant assembly.



GUODONG CHEN was born in 1983. He received the Ph.D. degree from the Harbin Institute of Technology, Harbin, China, in 2011. He is currently an Associate Professor with Soochow University. His research interests include robot vision and intelligent industrial robot.



HUI XU was born in 1989. He received the B.E. and M.S. degrees from the School of Mechanical and Electrical Engineering, Soochow University, Suzhou, China, in 2012 and 2015, respectively, where he is currently pursuing the Ph.D. degree in intelligent robot technology. His research interests include robot, and vision and motion planning.



ZHENG WANG was born in 1984. She received the Ph.D. degree from Fudan University, Shanghai, China, in 2017. She is currently an Associate Professor. Her research interests include vision-based robot control and robotics.